Eur Biophys J (2012) 41:483–489
DOI 10.1007/s00249-012-0803-y

BIOPHYSICS LETTER

EBSA
Biophysics in Europe

Effect of the A30P mutation on the structural dynamics of micelle-bound αSynuclein released in water: a molecular dynamics study

Prathit Chatterjee · Neelanjana Sengupta

Received: 14 January 2012 / Revised: 23 February 2012 / Accepted: 7 March 2012 / Published online: 24 March 2012

Abstract Atomistic molecular dynamics simulation has been used to probe the effect of the A30P mutation on the structural dynamics of micelle-bound, helical αSynuclein when released in an aqueous environment. On the timescales simulated, the effect of the mutation on the secondary structure is restricted to local changes close to the mutation site in the N-terminal helical domain. The changes are transient, and all residues except Lys23 recover their initial structure. The local behavior due to the mutation gives rise to a global difference in the A30P mutant in the form of a permanent kink in the N-terminal helical domain.

Keywords Alpha synuclein · A30P mutation · Molecular dynamics simulation · Structural persistence · Kink formation

Introduction

Spontaneous aggregation of alpha synuclein (αS), a ~14.5 kDa protein present in neuronal cytosol, is the causative factor of Parkinson's disease (Iwai et al. 1995). Although its physiological action is unclear, monomeric αS is involved in neurotransmitter release (Lotharius and Brundin 2002; Norris et al. 2004) and in ER/Golgi trafficking (Cooper et al. 2006), or is associated with synaptic vesicles (Cookson 2005; McLean et al. 2000). Residues 61–95 are associated with aggregates of the non-amyloid component (NAC) in Alzheimer's disease plaques (Uéda et al. 1993). The monomeric form is believed to have no stable tertiary structure in an aqueous environment, whereas it assumes helical conformations when bound to amphiphilic micelles and lipid bilayers (Chandra et al. 2003; Davidson et al. 1998; Eliezer et al. 2001; Uversky et al. 2001). In vivo, approximately 15 % of αS is membrane-bound at any given moment, and the seeding of aggregation of cytosolic αS has been found to be initiated by the membrane-bound form (Lee et al. 2002). It preferentially binds to anionic membranes but also binds to neutral membranes (Mihajlovic and Lazaridis 2008). Because, in vivo, αS co-exists in aqueous media with the lipid-bound form, it is plausible that helix↔coil↔β-sheet transitions could constitute important, early components of the fibrillogenesis pathway, understanding of which could help reveal the importance of helical or partially folded intermediates in amyloidogenesis (Abedini and Raleigh 2009; Dobson 1999; Hauser et al. 2011; Kelly 1998).

Early-onset Parkinson's disease has been linked to three point mutations (A30P, A53T, E46K) in αS (Krüger et al. 1998; Polymeropoulos et al. 1997; Zarranz et al. 2004). In vitro studies indicate that the rate of fibrillation increases with A53T and E46K (Conway et al. 1998; Greenbaum et al. 2005) and that A30P promotes formation of prefibrillar oligomeric species (Conway et al. 2000). NMR analysis suggests that A30P and A53T do not affect the protein's global structural properties except for some minor perturbation around the A30P mutation site (Bussell and Eliezer 2004). But analysis of C_α secondary shifts reveals that A30P mutation reduces the helical propensity and elongates the fibrillization lag phase (Bussell and Eliezer 2001, 2004).

Despite numerous studies, the mechanistic importance of mutations in affecting αS behavior remains incompletely

Electronic supplementary material The online version of this article (doi:10.1007/s00249-012-0803-y) contains supplementary material, which is available to authorized users.

P. Chatterjee · N. Sengupta (✉)
Physical Chemistry Division, National Chemical Laboratory, Pune 411008, India
e-mail: n.sengupta@ncl.res.in

understood. The A30P mutation is a particularly interesting case, because proline, usually found at helical ends, in turn regions, or at the edge strands of beta sheets, behaves as a structural disruptor when occurring mid-sequence in a protein (Barlow and Thornton 1988). In αS, this mutation has been found to cause several interesting alterations to the protein's intrinsic structural dynamics (Bussell and Eliezer 2004; Ulmer and Bax 2005). Experiments and simulations indicate that in a lipid environment it gives rise to destabilization upstream and downstream from the mutation site (Bussell and Eliezer 2004; Ulmer and Bax 2005), and reduces helical propensity and lipid binding affinity (Jensen et al. 1998; Jo et al. 2002; Perlmutter et al. 2009). The strong interactions of WT αS when bound to micelles are found to induce strain in the protein structure which is released with the A30P mutation (Ulmer and Bax 2005; Ulmer et al. 2005). However, it remains to be understood whether the strain is also present when the helical micelle-bound form is released into the aqueous environment, and the extent to which the A30P mutation affects the structural persistence of the WT form, hence reflecting the difference between the two variants in the early components of fibrillogenesis, as discussed earlier.

Starting with the micelle-bound conformation, we have compared the early structural evolution of the monomeric WT and A30P mutants of αS by using atomistic molecular dynamics (MD) simulation. Although neither form unfolds completely within the simulation time of 90 ns, our analysis reveals key differences in their intrinsic structural dynamics, attributable to the N-terminal region. The backbone RMSD of the A30P mutant attains a high but stable value at approximately 20 ns, whereas that of the WT protein continues to increase throughout the simulation. Our torsional angle-based structural persistence data indicate that unlike the WT, the first helical domain of the A30P undergoes a transient loss in secondary structure because of weakening of the backbone hydrogen-bonding network. The loss of helicity is localized, occurring at least five residues away from the mutation site toward the N-terminus, but gives rise to a kink-like feature that persists even after the secondary structure is recovered. Our results indicate that on release into the aqueous environment, the A30P form of the micelle-bound protein releases structural strain more easily than the WT form. We discuss the implications of our observations in the aggregation pathway of αS.

Computational methods

MD simulations

The micelle-bound form of αS (PDB entry 1XQ8) was the starting structure in our study (Ulmer et al. 2005). This structure comprises an N-terminal helical domain (Val3–Val37), a well-ordered extended linker (Leu38–Thr44), a C-terminal helical domain (Lys45–Thr92), another linker (Gly93–Lys97), and a highly disordered tail (Asp98–Ala140) (Ulmer et al. 2005). The tail region (residues 96–140) was truncated to study the enhanced fibrillization propensity (Crowther et al. 1998; Hoyer et al. 2004) while selecting the helical domains. The structure was mutated at position 30 with proline in the trans conformation to obtain the A30P form (Ulmer and Bax 2005). Four chloride counterions were added to neutralize each system, which were then solvated explicitly with approximately 9,000 TIP3P water molecules (Jorgensen et al. 1983). The box dimensions used for the systems measured approximately 60, 102, and 46 Å. The systems were simulated using the NAMD2.7 simulation package (Kalé et al. 1999) and the CHARMM22 all-atomic force field with CMAP correction (Mackerell 2004). The time step was taken to be 2 fs. Initially, energy minimizations of 15,000 steps were performed on the basis of the conjugate gradient method, following which the systems were simulated at a pressure of 1 atm. and a temperature of 310 K. Constant temperature was maintained using Langevin dynamics with a collision frequency of 1 ps^{-1}. The Nosé–Hoover Langevin piston (Feller et al. 1995) maintained constant pressure, and SHAKE (Ryckaert et al. 1977) was used to constrain the lengths of hydrogen bonds. Cutoffs of 12 Å were used with smooth truncation starting at 10 Å. Long-range electrostatics were calculated with particle mesh Ewald (PME) (Essmann et al. 1995). Ninety-nanosecond simulation trajectories were generated for both forms. VMD (Humphrey et al. 1996) was used for visualization.

Structural persistence

We define the structural persistence, P, to characterize the extent of secondary structure persistence of a chosen protein domain, relative to a reference structure. This variable is calculated as:

$$P = \frac{1}{N_{res}} \sum_{j=1}^{N_{res}} e^{-(\Delta\phi_j/\Delta\phi_{\max})} . e^{-(\Delta\psi_j/\Delta\psi_{\max})} \quad (1)$$

Here, $\Delta\phi_j$ and $\Delta\psi_j$ are, respectively, the changes in the ϕ and ψ torsional angles of the j'th residue over a reference structure, and the scaling factors $\Delta\phi_{\max}$ and $\Delta\psi_{\max}$ represent the maximum changes that can occur in the torsional angles in the Ramachandran diagram. The maximum value of the persistence, $P = 1$, is for a conformation whose secondary structure is completely unchanged relative to the reference. For a conformation in which nearly every residue undergoes the maximum change in the torsion angles, P is $\sim e^{-2}$. Lower values indicate less overall persistence

of secondary structure, and thus P is a measure of the global extent of structural disorder of the chosen domain compared with the reference structure.

Results and discussion

We present representative "snapshots" of the protein from the WT and A30P trajectories in Fig. 1, from which emerge several aspects of the structural evolution, and some interesting differences between the "global" behavior of WT and A30P monomers. First, the initial, micelle-bound structure does not seem to undergo extensive unfolding in water within the simulation timescale. Second, the loss in helicity seems to be transient and localized in small, contiguous domains within the N-terminal and C-terminal helical domains. Although no noticeable helicity loss is found in the N-terminal domain (residues Val3–Val37; henceforth referred to as N-helix) in the WT trajectory, transient "local" level helicity losses are noticed in the A30P trajectory. Closer inspection reveals that the helicity loss occurs away from the site of the mutation, toward the N-terminus (i.e. "upstream"), and is recovered at the latter part of the trajectory. For the C-terminal helical domain (Lys45–Thr92; henceforth referred to as C-helix), there seem to be transient helical losses to a smaller extent for both mutants. The snapshots also suggest that the helical domains bend and form distinct kinks. The N-helix forms distinct kinks only in the A30P trajectory, which persists after the helicity has been recovered. On the other hand, bends in the C-helix appear in both trajectories, and seem to be more transient in nature.

In Fig. 2, we have plotted the root-mean-squared deviations (RMSD) of backbone atoms of the WT and A30P proteins obtained over the simulations, relative to the initial structure. The RMSD for the WT protein rises steadily over the 90 ns, indicating a gradual but steady change in structural evolution. On the other hand, the RMSD for the A30P variant initially rises rapidly (by nearly 10 Å), followed by a nearly 70 ns period of marked stability. Thus, on the whole, the A30P variant has an initial phase wherein it undergoes a rapid structural change, and the resulting stable structure persists for longer. The mean RMSD value of the WT over the entire simulation trajectory is 10.5 (±3.2) Å. For the A30P, the mean value over the first 20 ns is 9.7 (±3.3) Å; it is 12.4 (±0.9) Å for the latter part.

To quantify the extent of structural persistence of the micelle-bound structure, and to probe the effect of the proline mutation on evolution of the structure at the "global" and "local" scales, we obtained the persistence, P, as defined by Eq. (1), for different domains along the trajectories, with the original structure as the reference.

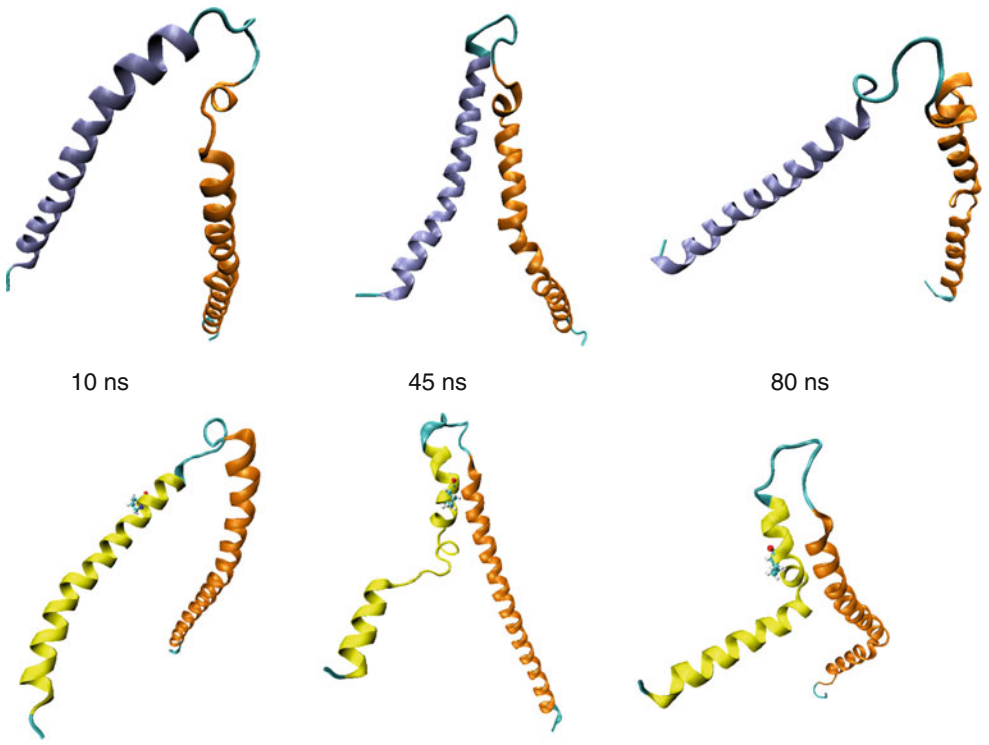

Fig. 1 Snapshots of the WT (*upper row*) and A30P (*lower row*) variants taken at 10, 45, and 80 ns of the respective trajectories. The N-helices of WT and A30P are shown in *blue*, and *yellow*, respectively. The proline mutation in A30P is marked with CPK representation. C-helices are shown in *orange*

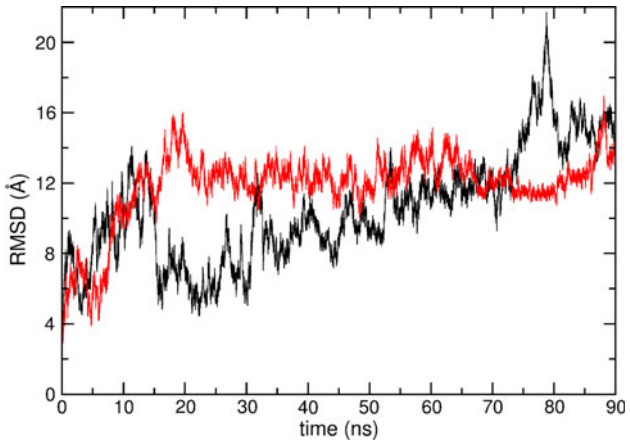

Fig. 2 Evolution of the backbone RMSDs of the WT (*in black*) and A30P (*in red*) as a function of simulation time

In Fig. 3, we show *P* obtained for the whole protein, and individually for the N and C-helices. When considering the entire protein, *P* consistently has a high value (0.85 or more) throughout the simulation time. Thus, at the scale of the full protein, the overall structural integrity of both the whole WT and A30P systems is largely maintained. At the level of the individual helical domains, *P* remains high, but interesting differences between WT and A30P are observed. For the N-helix in WT, the mean value of *P* fluctuates over the simulation, and is 0.93 (±0.01). For the helix in A30P, on the other hand, there is a dramatic drop between 25 and 30 ns, which recovers after 65 ns. We note that the drop commences at approximately the same time as the RMSD value attains the high, stable value, and is coincident with the onset of the upstream helical losses and bending in the N-helix. The mean *P* values between 0–25, 30–60, and 70–90 ns for the A30P N-helix are 0.93 (±0.01), 0.82 (±0.04), and 0.91 (±0.01), respectively. For the C-helix, *P* follows a pattern that is independent of the N-helix in both trajectories. Whereas *P* for this helix is high for both systems (∼0.9 or more), the values are slightly higher for the A30P, but merge during the last ∼25 ns. Thus, the slightly higher whole protein *P* of A30P over the WT during the first ∼20 ns should be attributable to unfolding differences in the C-terminal domain; the fall and subsequent merging with the value of WT at ∼25 ns is because of significant unfolding in the N-terminal domain.

To elucidate the local, residue-level unfolding behavior because of the mutation, we recalculated *P* for three-residue groups in the N and C-helices. In Figs. ESM-1 and ESM-2 in the *Supplementary Material*, we compare *P* for groups within the N-helix from the WT and A30P trajectories. Comparison with the evolution of *P* for the entire N-helix confirms that the disorder due to the mutation arises upstream, toward the N-terminus. Residue groups downstream ($K_{32}TK_{34}$) and at the mutation site ($A_{29}PG_{31}$) have high *P* values (∼0.95) throughout the simulation. The domain-level drop in *P* observed for the entire N-helix at 25 ns is clearly found to be due to residue groups $K_{23}QG_{25}$, $A_{17}AA_{19}$, and $G_{14}VV_{16}$. Groups $V_{26}AE_{28}$, $E_{20}KT_{22}$ and $A_{11}KE_{13}$ have high but fluctuating *P* values with no evident correlations with the domain-level trend. Notably, although *P* is recovered for $A_{17}AA_{19}$ and $G_{14}VV_{16}$, the decrease in *P* persists for $K_{23}QG_{25}$ for the remaining simulation time; this is, thus, the only domain

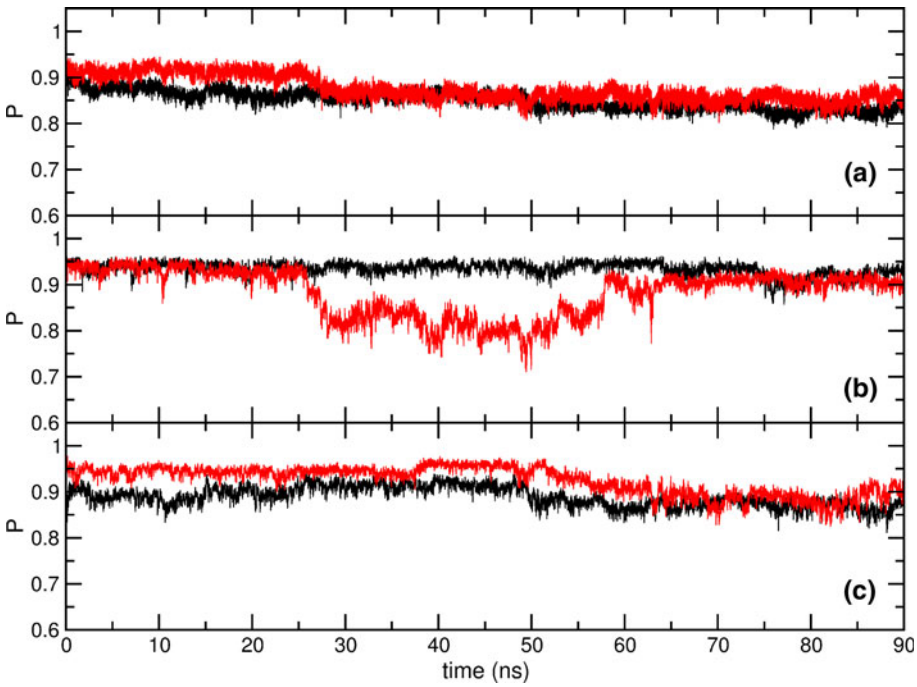

Fig. 3 Plots of the persistence, *P*, of the WT (*in black*) and A30P (*in red*) variants as a function of simulation time, shown for *a* the whole peptide segments, *b* the N-helix, and *c* the C-helix

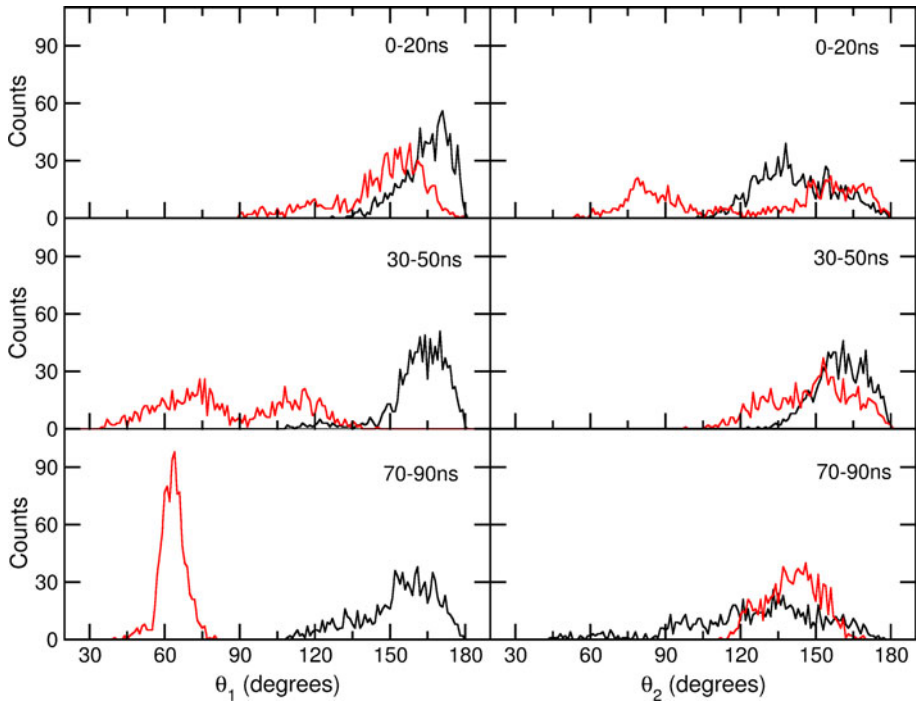

Fig. 4 Histograms of bend angles θ_1 and θ_2 for the WT (*in black*) and A30P (*in red*) variants, taken over 0–20, 30–50 and 70–90 ns

with a permanent secondary structure change due to the mutation. Further, as backbone hydrogen bonding networks in alpha helices are of the type $i \leftarrow i+4$ (the arrow indicating the direction of hydrogen bond), the absence of the (NH) group at the location of the mutation should cause a cascading weakening of structural hydrogen bonds towards the N-terminus. Individually, we find that Lys23 has the greatest "permanent" drop in P at 25 ns (by approx. 0.6; data not shown); P for other residues recovers close to 65 ns. On the other hand, "local" P values in the C-terminal domain are not clearly different; transient helical unfolding from Gly67–Val74 is noticed in both the variants (Figs. ESM-3, 4).

To probe the propensity for helical bending, we evaluated the bend angles in the N-helix, θ_1 (defined as the angle at Lys23, i.e. between Val3–Thr22 and Gln24–Val37) and in the C-helix, θ_2 (the angle made by the residue stretches Lys45–Val66 and Thr75–Val95, for which structural persistence is higher). In Fig. 4, we have compared histograms of θ_1 and θ_2 over segments of the simulation trajectory chosen when P for the N-helix in A30P did not undergo significant changes (0–20, 30–50, and 70–90 ns). For the WT trajectory, the distribution of θ_1 peaks between 160° and 170°, and does not change significantly during the time periods chosen. However, for A30P, this distribution shows a clear shift in the peak maximum as time progresses. Within the first 20 ns, most conformations correspond to a nearly unbent N-helix, with a distinct peak in θ_1 at $\sim$160°, and a smaller peak at $\sim$120°. Between 30 and 50 ns, we find distinct shifts in the peak, with significant contributions from "kinked" conformations where θ_1 peaks at $\sim$75° and $\sim$115°. In the last 20 ns of the simulation, the distribution peaks strongly at $\sim$65°, showing a distinct tendency of the first helical domain to bend in the A30P trajectory.

The distributions for the bending angle θ_2, on the other hand, are not clearly different between the simulated WT and A30P systems. For WT, the initial peak (at $\sim$140°) for 0–20 ns shifts towards a slightly *higher* value ($\sim$160°) between 30 and 50 ns. For the last 20 ns, the distribution (which peaks at $\sim$130°) is broader, with no clear preference for either the straightened or the bent form. For A30P, the first 20 ns correspond to two distinct peaks (at $\sim$80° and $\sim$160°). However, between 50 and 70 ns, the peak at $\sim$80° is lost, signifying a decrease in the bent structures. For the last 20 ns, the distribution actually contracts around the peak of $\sim$140°, also revealing a final preference for neither straight nor bent structure. Therefore, we find no clear correlation between the trends of θ_1 and θ_2.

We point out here that for the A30P trajectory, the initial drop and subsequent stability in θ_1 (Fig. ESM-5) is reminiscent of the temporal pattern of the backbone RMSD. Thus, the kink formation in the first helical domain is the main structural effect of the mutation at the "global" level. This is confirmed by evaluating the backbone RMSDs individually for the N and C-helices (Fig. ESM-6).

Conclusions

We have reported the effect of the A30P mutation on the early structural dynamics of the micelle-bound structure

of αS when released in an aqueous environment. Globally, high structural persistence is observed for both the WT and mutant forms on nanosecond timescales. However, the A30P mutation is found to cause partial unfolding in the N-terminal domain. The loss of helicity in this domain is transient, and all residues except Lys23, located seven residues upstream from the site of the mutation, fully regain their helical conformation. We find that the sudden drop in the persistence for the N-helix of A30P is nearly commensurate with the onset of a kink-like feature. The kink formation is stable, and does not reverse with recovery of overall helicity for most residues. We find that the sharp increase in backbone RMSD of the A30P trajectory at $\sim$20 ns is commensurate with a drop in θ_1. Unlike the persistence, the starting value of θ_1 is not recovered. Thus, the higher, stable RMSD in the A30P variant in the latter part of the trajectory is because of the formation of a stable kink in the N-helix. This is confirmed by comparing the backbone RMSD plots of the individual helices with θ_1.

It is noted here that micelle-bound monomeric αS is reported to be a strained structure (Ulmer and Bax 2005), and the proline mutation has been shown to be of key importance in the release of strain of the A30P form by either upstream or downstream helical destabilization (Bussell and Eliezer 2004; Ulmer and Bax 2005). Our MD simulation results suggest that in an aqueous environment the transient structural disorder upstream from the mutation site and the permanent kink formation in the N-helix of the A30P could be a key mechanism of strain release. In comparison, the extent of strain released in the C-helix should be comparable in both mutant varieties. Continuing studies by our group will focus on relationships among thermodynamic aspects of the structural changes and associated strain release. As a preliminary analysis, we have compared temporal patterns of the energies of backbone hydrogen-bonding network of the N and C-helices for both trajectories (Fig. ESM-7). The data show that the A30P mutation transiently weakens the hydrogen-bonding network associated with the structure of the N-helix; the magnitude of the destabilization from 25 to 60 ns is greater than 400 kcal mol^{-1}. Comparison with the P for the N-helix suggests that entropic effects have an important role in the helical unfolding. We note that the hydrogen-bonding network in the C-helix remains unaffected, reiterating that structural dynamics of the two domains are independent within the timescales simulated.

Destabilization of the backbone hydrogen-bonding network in the A30P mutant could be one of the key reasons for recovery of the helical structure on the timescales simulated. However, because all mutant forms of monomeric αS are experimentally found to be intrinsically unstructured in water, the helical reformation itself should be transient when longer timescales are considered. Therefore, the unfolding pathway of the protein may involve populations of structures of different helicity. Longer trajectories (possibly up to the microsecond time range or longer) will be required to reveal in detail the interplay between the different thermodynamic and kinetic factors that eventually lead to total unfolding of the peptide in an aqueous environment. Further, longer simulations involving multiple monomers will be able to demonstrate how structural features arising because of the mutations and encountered along the unfolding pathway can modulate the self-assembly process. For example, the kink in the A30P trajectory may affect the relative proximities, and thereby the interaction strengths, of key residues that participate in the self-assembly mechanism.

Single-point mutations in the amino acid sequence of αS are responsible for significant alterations to the protein's structural behavior and self-assembly. Clearer, molecular level understanding of the structural dynamics underlying the protein's mutant forms is essential for understanding their complex aggregation behavior. Our results revealing important differences between the intrinsic structural dynamics of the A30P variant and the WT form are, therefore, relevant in describing the very early steps of self assembly of αS.

Acknowledgments PC acknowledges CSIR for a Junior Research Fellowship. NS acknowledges funds from DST-India (fast track grant GAP280526), funds and computing resources from the Centre of Excellence in Scientific Computing at NCL, and computing resources from CDAC, Pune.

References

Abedini A, Raleigh DP (2009) A role for helical intermediates in amyloid formation by natively unfolded polypeptides? Phys Biol 6:015005

Barlow DJ, Thornton JM (1988) Helix geometry in proteins. J Mol Biol 201:601–619

Bussell R, Eliezer D (2001) Residual structure and dynamics in Parkinson's disease-associated mutants of αSynuclein. J Biol Chem 276:45996–46003

Bussell R, Eliezer D (2004) Effects of Parkinson's disease-linked mutations on the structure of lipid-associated αSynuclein. Biochemistry 43:4810–4818

Chandra S, Chen X, Rizo J, Jahn R, Südhof TC (2003) A broken α-helix in folded αSynuclein. J Biol Chem 278:15313–15318

Conway KA, Harper JD, Lansbury PT (1998) Accelerated in vitro fibril formation by a mutant αSynuclein linked to early-onset Parkinson's disease. Nat Med 4:1318–1320

Conway KA, Lee S-J, Rochet J-C, Ding TT, Williamson RE, Lansbury PT (2000) Acceleration of oligomerization, not fibrillization, is a shared property of both αSynuclein mutations linked to early-onset Parkinson's disease: implications for pathogenesis and therapy. Proc Nat Acad Sci USA 97:571–576

Cookson MR (2005) The biochemistry of Parkinson's disease. Ann Rev Bio 74:29–52

Cooper AA, Gitler AD, Cashikar A, Haynes CM, Hill KJ, Bhullar B, Liu K, Xu K, Strathearn KE, Liu F, Cao S, Caldwell KA, Caldwell GA, Marsischky G, Kolodner RD, LaBaer J, Rochet J-C, Bonini NM, Lindquist S (2006) αSynuclein blocks ER-Golgi traffic and Rab1 rescues neuron loss in Parkinson's models. Science 313:324–328

Crowther RA, Jakes R, Spillantini MG, Goedert M (1998) Synthetic filaments assembled from C-terminally truncated αSynuclein. FEBS Lett 436:309–312

Davidson WS, Jonas A, Clayton DF, George JM (1998) Stabilization of αSynuclein secondary structure upon binding to synthetic membranes. J Biol Chem 273:9443–9449

Dobson CM (1999) Protein misfolding, evolution and disease. Trends Biochem Sci 24:329–332

Eliezer D, Kutluay E, Bussell R Jr, Browne G (2001) Conformational properties of αSynuclein in its free and lipid-associated states. J Mol Biol 307:1061–1073

Essmann U, Perera L, Berkowitz ML, Darden T, Lee H, Pedersen LG (1995) A smooth particle mesh Ewald method. J Chem Phys 103:8577–8593

Feller SE, Zhang Y, Pastor RW, Brooks BR (1995) Constant pressure molecular dynamics simulation: the Langevin piston method. J Chem Phys 103:4613–4621

Greenbaum EA, Graves CL, Mishizen-Eberz AJ, Lupoli MA, Lynch DR, Englander SW, Axelsen PH, Giasson BI (2005) The E46K Mutation in αSynuclein increases amyloid fibril formation. J Biol Chem 280:7800–7807

Hauser CAE, Deng R, Mishra A, Loo Y, Khoe U, Zhuang F, Cheong DW, Accardo A, Sullivan MB, Riekel C, Ying JY, Hauser UA (2011) Natural tri-to hexapeptides self-assemble in water to amyloid β-type fiber aggregates by unexpected α-helical intermediate structures. Proc Nat Acad Sci USA 108:1361–1366

Hoyer W, Cherny D, Subramaniam V, Jovin TM (2004) Impact of the acidic C-terminal region comprising amino acids 109–140 on αSynuclein aggregation in vitro. Biochemistry 43:16233–16242

Humphrey W, Dalke A, Schulten K (1996) VMD: visual molecular dynamics. J Mol Graph 14:33–38

Iwai A, Masliah E, Yoshimoto M, Ge N, Flanagan L, Rohan de Silva HA, Kittel A, Saitoh T (1995) The precursor protein of non-Aβ component of Alzheimer's disease amyloid is a presynaptic protein of the central nervous system. Neuron 14:467–475

Jensen PH, Nielsen MS, Jakes R, Dotti CG, Goedert M (1998) Binding of αSynuclein to brain vesicles is abolished by familial Parkinson's disease mutation. J Biol Chem 273:26292–26294

Jo E, Fuller N, Rand RP, George-Hyslop P, Fraser PE (2002) Defective membrane interactions of familial Parkinson's disease mutant A30P αSynuclein. J Mol Biol 315:799–807

Jorgensen WL, Chandrasekhar J, Madura JD, Impey RW, Klein ML (1983) Comparison of simple potential functions for simulating liquid water. J Chem Phys 79:926–935

Kalé L, Skeel R, Bhandarkar M, Brunner R, Gursoy A, Krawetz N, Phillips J, Shinozaki A, Varadarajan K, Schulten K (1999) NAMD2: greater scalability for parallel molecular dynamics. J Comput Phys 151:283–312

Kelly JW (1998) The alternative conformations of amyloidogenic proteins and their multi-step assembly pathways. Curr Opin Struct Biol 8:101–106

Krüger R, Kuhn W, Müller T, Woitalla D, Graeber M, Kösel S, Przuntek H, Epplen JT, Schöls L, Riess O (1998) Ala30Pro mutation in the gene encoding αSynuclein in Parkinson's disease. Nat Gen 18:106–108

Lee H-J, Choi C, Lee S-J (2002) Membrane-bound αSynuclein has a high aggregation propensity and the ability to seed the aggregation of the cytosolic form. J Biol Chem 277:671–678

Lotharius J, Brundin P (2002) Pathogenesis of Parkinson's disease: dopamine, vesicles and αSynuclein. Nat Rev Neurosci 3:932–942

Mackerell AD (2004) Empirical force fields for biological macromolecules: overview and issues. J Comput Chem 25:1584–1604

McLean PJ, Kawamata H, Ribich S, Hyman BT (2000) Membrane association and protein conformation of αSynuclein in intact neurons. J Biol Chem 275:8812–8816

Mihajlovic M, Lazaridis T (2008) Membrane-bound structure and energetics of αSynuclein. Proteins Struct Funct Bioinform 70:761–778

Norris EH, Giasson BI, Lee VMY, Gerald PS (2004) αSynuclein: normal function and role in neurodegenerative diseases. Curr Top Dev Biol 60:17–54

Perlmutter JD, Braun AR, Sachs JN (2009) Curvature dynamics of αSynuclein familial Parkinson disease mutants. J Biol Chem 284:7177–7189

Polymeropoulos MH, Lavedan C, Leroy E, Ide SE, Dehejia A, Dutra A, Pike B, Root H, Rubenstein J, Boyer R, Stenroos ES, Chandrasekharappa S, Athanassiadou A, Papapetropoulos T, Johnson WG, Lazzarini AM, Duvoisin RC, Di Iorio G, Golbe LI, Nussbaum RL (1997) Mutation in the αSynuclein gene identified in families with Parkinson's disease. Science 276:2045–2047

Ryckaert J-P, Ciccotti G, Berendsen HJC (1977) Numerical integration of the cartesian equations of motion of a system with constraints: molecular dynamics of n-alkanes. J Comput Phys 23:327–341

Uéda K, Fukushima H, Masliah E, Xia Y, Iwai A, Yoshimoto M, Otero DA, Kondo J, Ihara Y, Saitoh T (1993) Molecular cloning of cDNA encoding an unrecognized component of amyloid in Alzheimer disease. Proc Nat Acad Sci USA 90:11282–11286

Ulmer TS, Bax A (2005) Comparison of structure and dynamics of micelle-bound human αSynuclein and Parkinson disease variants. J Biol Chem 280:43179–43187

Ulmer TS, Bax A, Cole NB, Nussbaum RL (2005) Structure and dynamics of micelle-bound human αSynuclein. J Biol Chem 280:9595–9603

Uversky VN, Li J, Fink AL (2001) Evidence for a partially folded intermediate in αSynuclein fibril formation. J Biol Chem 276:10737–10744

Zarranz JJ, Alegre J, Gómez-Esteban JC, Lezcano E, Ros R, Ampuero I, Vidal Ld, Hoenicka J, Rodriguez O, Atarés Ba, Llorens Vn, Gomez Tortosa E, del Ser T, Muňoz DG, de Yebenes JG (2004) The new mutation, E46K, of αSynuclein causes Parkinson and Lewy body dementia. Ann Neurol 55:164–173